Pressure Mapping from Flow Imaging: Enhancing Computation of the Viscous Term Through Velocity Reconstruction in Near-Wall Regions

Fabrizio Donati[1], David A. Nordsletten[1], Nicolas P. Smith[1,2], Pablo Lamata[1,3].

Abstract— **Although being small compared to inertial acceleration, viscous component of the pressure gradient has recently emerged as a potential biomarker for aortic disease conditions including aortic valve stenosis. However, as it involves the computation of second order derivatives and viscous dissipation is locally higher in the near-wall region of the larger vessels, where the lowest local signal-to-noise ratios are encountered, the estimation process from medical image velocity data through mathematical models is highly challenging. We propose a fully automatic framework to recover the laminar viscous pressure gradient through reconstruction of the velocity vector field in the aortic boundary region. An in-silico study is conducted and the pressure drop is computed solving a Poisson problem on pressure using both a reconstructed and non-reconstructed velocity profile near the vessel walls, showing a global improvement of performance with the enhanced method.**

I. INTRODUCTION

Aortic valve stenosis (AVS) is a common cardiovascular disease in the Western world, with an alarming average of less than 4 years survival without intervention [1]. In moderate-to-severe AVS, calcification due to age or congenital factors may lead to inefficient opening of the aortic valve and partial obstruction of the outflow. In this condition heart workload during systolic phase is therefore increased and the left ventricular (LV) compartment may undergo fatal failure. Transvalvular pressure gradient has a key role in the assessment of AVS severity, helping in the management of patients that are candidates to receive surgical repair [3], [7].

Gold standard for pressure measurement is catheterization, which however is an invasive procedure and inevitably contaminated by the physical presence of the catheter [4], [13]. In the last decades, non-invasive pressure estimation methods using medical imaging have been proposed. Specifically, four-dimensional (time-resolved 3D) flow phase-contrast magnetic resonance imaging (PC-MRI) data provides an enhanced description of the hemodynamics and flow patterns in the vasculature, and mathematical models have been used to derive pressure from the acquired flow field [2], [5].

In this context the Poisson pressure equation (PPE) formulation is commonly used [6], [8], [11], as it minimizes the issues of high sensitivity to boundary conditions with the Navier-Stokes' equations original form. More recently a finite-element method (FEM) to the solution of the PPE described in [8] has shown that, if incompressibility is enforced, the weak form of the equation is reduced to a simple balance between volume integrals, thus completely removing the boundary conditions on pressure gradient, which are not readily available. This development is critical for a reliable estimation of viscous component of pressure, with the first results reported in [9].

Nevertheless, the challenges in the computation of viscous pressure have not been properly addressed. The laminar viscous effects are higher in the near-wall region, and computations of pressure are commonly performed only in the central part of the lumen, where the inertial effects predominate [8]. Therefore, major viscous effects happening at the vessel boundary are not captured with a mesh that does not include this part of the domain. Additionally, flow data at the boundary region shows characteristics that compromise the computation of relative pressure, like a low signal-to-noise ratio (SNR), low spatial resolution, and partial volume effects.

In this study we propose a finite-element approach to PPE to compute the laminar viscous pressure drop from PC-MRI data. Our motivation is the hypothesis that viscous effects represent a potential biomarker to stratify disease, as mechanical energy dissipation reflects directly inefficiencies of the heart pumping mechanism. The method achieves the integration of the boundary region by an automatic fitting of a smooth tubular computational mesh to the segmentation domain. Low-SNR and data issues are addressed by the reconstruction of the velocity profile via a Stokes-driven degrees of freedom repopulation in the near-wall region. We then investigate the requirements of segmentation accuracy of the input PC-MRI data, and the impact of different levels of SNR to the solution.

II. METHODS AND MATERIALS

The method for the estimation of relative pressure consists of three main steps: (A) generation of the computational mesh, (B) near-wall velocity reconstruction, and (C) pressure estimation, as described in the following subsections. The performance is evaluated in an in-silico dataset, where the proposed enhanced method is compared to a direct computation (without velocity reconstruction) from (D) PC-MRI data synthetized with different levels of SNR.

A. Generation of the computational mesh

The computational mesh is generated by (1) an automatic thresholding segmentation of the velocity magnitude image,

[1]Department of Biomedical Engineering, Division of Imaging Sciences and Biomedical Engineering, King's College London, Kings Health Partners, St. Thomas' Hospital, London, SE1 7EH, United Kingdom.
[2]Faculty of Engineering, The University of Auckland, New Zealand.
[3]Department of Computer Sciences, Computing Laboratory, University of Oxford.

978-1-4244-7929-0/14/$26.00 ©2014 IEEE

(2) the construction of a suitable mesh template with user-defined topology, and (3) a warping process of the template to the segmentation domain by an image-registration solution. In the design of the template, the mesh topology is chosen as a cylinder with concentric layers of elements in order to allow the definition of the boundary region as a subset of layers of elements. Second-order hexahedral elements are chosen in the FEM discretization. Higher resolution is imposed in the near-wall region, while in the inner core region nodes coarseness is acceptable. The mesh personalization algorithm recently proposed by Lamata et. al [10] is adapted to this problem, and achieves the fitting of the template into the segmentation domain with sub-voxel accuracy.

Reconstruction of the velocity field is performed in the near-wall region solely. Therefore, the computational mesh is divided in two regions, corresponding to a *trusted* high-SNR and an *untrusted* low-SNR region (near-wall). A choice of a number of 8 computational elements in the transmural direction, corresponding to $\approx 25\%$ of the lumen diameter, is fixed in this study.

B. Near-wall velocity reconstruction

At this point, a domain separation is performed, based on the local SNR level, which is high in the core region of the flow field (where mean velocity is high) and is low at the boundaries, where a clear distinction between true signal and noise is difficult to assess. Based on that, hexahedral elements are labelled either as part of the core or bore region. Image registration allows for the interpolation of velocity from the PC-MRI on the boundary nodes of the bore region. A cubic interpolation scheme is chosen to define velocity at the required nodes of the warped mesh through the MATLAB build-in function *interp3*. This is necessary to define the boundary conditions on the internal boundary nodes in order to solve for velocity in the near-wall region on a finer grid. External nodes velocity values are set to 0, while boundary conditions on inlet and outlet nodes for the warped mesh are provided in the form of a force constraint. A Lagrange multiplier approach is adopted here, forcing velocity on those nodes to match data-derived velocity depending on the relaxation factor k. Higher values for this parameter imply stronger constraint of the velocity boundary conditions at the inlet/outlet of the warped mesh. Velocity reconstruction is obtained through solution of a Stokes' problem in this region, defined assuming viscous forces predominant on convective forces.

C. Pressure estimation

The estimation of relative pressure is performed following the methodology described in [8]. Pressure gradient is the response of a fluid system to inertial and viscous stresses and volume forces. Inertial effects are driven by acceleration due to the pulsatile nature of the blood flow and acceleration due to the morphology of the vasculature, which are respectively known as *transient* and *convective* acceleration. *Viscous* effects account for the mechanical dissipation that flow experiences because of laminar friction between neighbouring laminae, consequently being strictly related to inefficiency of the heart pump. *Volume* forces englobe gravitational acceleration and can be therefore neglected in this context. Navier-Stokes' system of equations provides an accurate description of this force balance,

$$-\nabla p = \overbrace{\underbrace{\rho\frac{\partial \mathbf{u}}{\partial t}}_{transient} + \underbrace{\rho\left(\mathbf{u}\cdot\nabla\right)\mathbf{u}}_{convective}}^{inertial} + \underbrace{\mu\Delta\mathbf{u}}_{viscous} + \underbrace{\mathbf{f}}_{volume}. \quad (1)$$

PPE is derived taking the divergence of the right-hand and left-hand side, thus simplifying the force balance to,

$$\Delta p = \nabla\cdot\mathbf{b}, \quad (2)$$

where the laplacian of pressure is now an explicit function of the velocity field derived from the image domain, enclosed in the divergence of the source term $\mathbf{b}$,

$$\mathbf{b} = \mu\Delta\mathbf{u} - \rho\left(\frac{\partial \mathbf{u}}{\partial t} + \left(\mathbf{u}\cdot\nabla\right)\mathbf{u}\right). \quad (3)$$

Transformation into the weak form reduces the PPE to a balance between volume integrals, with boundary conditions on pressure gradients being removed if incompressibility is assumed,

$$\int_\Omega \nabla p\cdot\nabla q\, d\Omega = \int_\Omega \mathbf{b}\cdot\nabla q\, d\Omega, \quad (4)$$

where the test function $q \in H^1(\Omega)$ is introduced. Then, a Galerkin approach is used to discretize the equation and the finite-element implementation is performed using quadratic Lagrangian basis functions, to allow second derivatives to be captured correctly.

The method we propose is aimed at improving the computation of the laminar viscous pressure gradient. Therefore, in the following we refer to pressure gradient as driven by the viscous stress solely, thus reducing the source term to,

$$\Delta p_{viscous} = \nabla\cdot\mu\Delta\mathbf{u}. \quad (5)$$

We compare the Stokes-enhanced PPE (SePPE) approach with a direct computation from PC-MRI data (DPPE) in terms of the pressure gradient percentage relative error defined as,

$$\varepsilon_{pg} = \frac{\frac{\overline{p}_{inlet} - \overline{p}_{outlet}}{L} - pg_{HP}}{pg_{HP}} \times 100. \quad (6)$$

Here, the pressure gradient is defined as the ratio between the difference of inlet and outlet mean pressures over the approximate length of the fitted geometry L and pg_{HP} is the analytic pressure gradient from the Hagen-Poiseuille theory. We investigate the sensitivity of the method to the detected lumen, defining the lumen detection error,

$$\varepsilon_\phi = \frac{\phi - \phi_{true}}{\phi_{true}} \times 100, \quad (7)$$

where the true lumen ϕ_{true} and the computed lumen ϕ are defined respectively as the radius of the analytic pipe and

the average of radii estimates resulting from a circle-fitting procedure operated at each cross-section of the fitted mesh. We assess the accuracy of the method as a function of the amount of trusted data from the image domain, defining the *Trusted Data Index* (TDI) as the ratio between the radius of the core region (high local SNR, thus reliable data from image) and the computed lumen,

$$\mathrm{TDI} = \frac{R_{trusted}}{\phi}. \tag{8}$$

A brief schematic of the basics behind the SePPE method is presented in Fig. 1. For the sake of completeness, a comparison between typical velocity profiles obtained using a DPPE and a SePPE approach following image-driven mesh personalization is shown in Fig. 2.

D. Test data: synthesis of PC-MRI data

PC-MRI data acquisition is reproduced in order to have full control of the noise level. An analytic 3D Hagen-Poiseuille flow in a cylindrical straight pipe, where an analytic ground truth solution is available for the pressure distribution, is chosen for the study. Simulated Gaussian noise in physiological range is added at the stage of mimicking the image acquisition, having the control parameter SNR defined as,

$$SNR = \frac{\mu}{\sigma},$$

where μ is the mean value of the flow field velocity magnitude and σ the standard deviation of the noise. Automatic segmentation of the output image is allowed by a thresholding criterion on the voxels' velocity magnitude v_S.

III. RESULTS

(i) Preliminary validation on boundary parameters

We performed preliminary tests to assess the impact of two crucial factors in the set up of the near-wall velocity reconstruction problem: the *image data reliability* and the *boundary region width*, respectively set by the relaxation constant k and TDI. Results showed low sensitivity of the pressure gradient relative error to k. Higher accuracy was

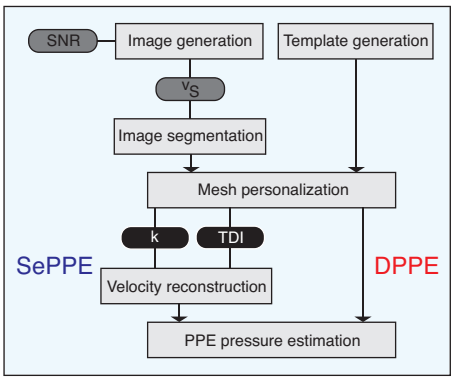

Fig. 1. Workflow from mesh personalization over near-wall velocity reconstruction to viscous relative pressure estimation. Image personalization parameters (dark grey background) and SePPE parameters (black background).

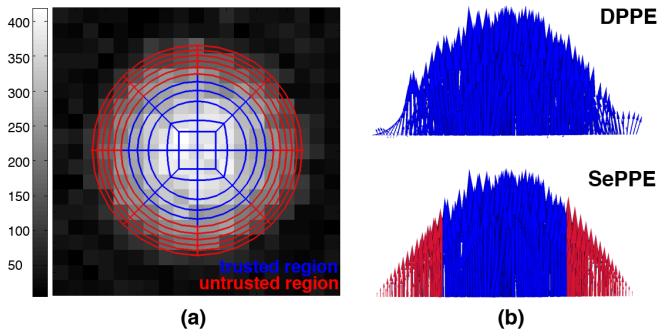

Fig. 2. Schematics of the velocity reconstruction process. Mesh fitting to segmented image with trusted/untrusted region separation (a). In plane velocity profile without velocity reconstruction (DPPE) and with velocity reconstruction (SePPE) (b).

however achieved with k in the range $\left[10^1 - 10^5\right]$, which translates into weaker boundary conditions for the inlet/outlet nodes' velocity. Therefore, $k = 10^3$ was used for the remainder of the study. Representative tests were performed with different amount of SNR within the physiological range $[5 - 15]$. As expected, SePPE performed better with decreasing TDI, showing a monotonically decreasing ε_{pg} as the trusted region from the image domain was reduced. Subsequently, we assessed the performance of SePPE against DPPE method as a function of the computed lumen ϕ.

(ii) Sensitivity of the pressure gradient to computed lumen

Fig. 3 illustrates that SePPE outperforms DPPE throughout all the detected lumens considered. For both methods, an underestimation of vessel diameter introduces an amplification of the pressure gradient, and vice-versa. A direct computation of velocity gradients relying solely on the data, without reconstruction of the boundary layer, causes an underestimation of the pressure gradient. Pressure drop is captured with good accuracy with the SePPE approach if $-2.5\% < \varepsilon_\phi < 2.5\%$ ($\approx 15\%$ vs $\approx -45\%$ in cases where lumen is underestimated, $\approx 5\%$ vs $\approx 50\%$ if overestimated). Performance of the method is again acceptable with moderate-to-high lumen overestimation ($\approx 20\%$ and $\approx 40\%$). Finally, the accuracy of both methods slightly drops when the true lumen is moderately underestimated, with SePPE overestimating the pressure gradient and DPPE underestimating it.

(iii) Sensitivity of the pressure gradient to SNR and v_S

Both methods were applied to the reconstructed geometry of the analytic in-silico pipe, assigning a fixed TDI ≈ 0.5. The combined effects of SNR and v_S were analyzed, to investigate the strong impact they have on the image domain generation and in turn on the pressure solution. SNR was varied again in the range $[5 - 15]$, along with the v_S in the range $[5\% - 15\%]$ of the analytically defined peak velocity. Every test was run 20 times and relative error was averaged to avoid random noise variability of results.

The pressure drop relative error provided by the SePPE approach is considerably lower than the DPPE one, when

physiologically relevant noise and segmentation threshold are considered (highlighted by rectangle in red, Fig. 4). Both methods perform poorly in case of high level of noise, whereas for the highest SNR proposed both methods are consistently accurate.

IV. DISCUSSION

We have proposed an automatic method to recover the laminar viscous pressure drop, and shown that the reconstruction of velocity fields in the boundary layer improves the results.

Laminar viscous dissipation is greatest at the boundary of the lumen, and this is where the SNR is worse in PC-MRI data. Results illustrate how the boundary layer reconstruction reduces the error in viscous pressure computation irrespective of the lumen segmentation error (Fig. 3). This study also highlights the requirement of segmentation errors less than a 2.5% in the estimation of lumen diameter in order to have an accurate laminar viscous pressure estimation (error $< 15\%$). Note that acquisitions typically have 8 to 9 voxels across the diameter of the aorta, and therefore there is a need of sub-voxel accuracy in lumen segmentation. This level of segmentation accuracy, also accounting for the displacement of the aorta, has been reported to be possible using implicit geometric models [12]. Results also illustrate that the method is robust to the choice of the relaxation constant needed for the reconstruction of the velocity field, and that different levels of SNR will introduce different optimal choices of the threshold to define the domain of computation.

The main limitation of this study lies in the hypothesized Hagen-Poiseuille velocity profile imposed in the in-silico model, which is not representative of physiological aortic flows. More specifically, this flow regime neglects the inertial effects of blood. Future works will address this issue by the simulation of the complete Navier-Stokes equations for the reconstruction of the boundary layer.

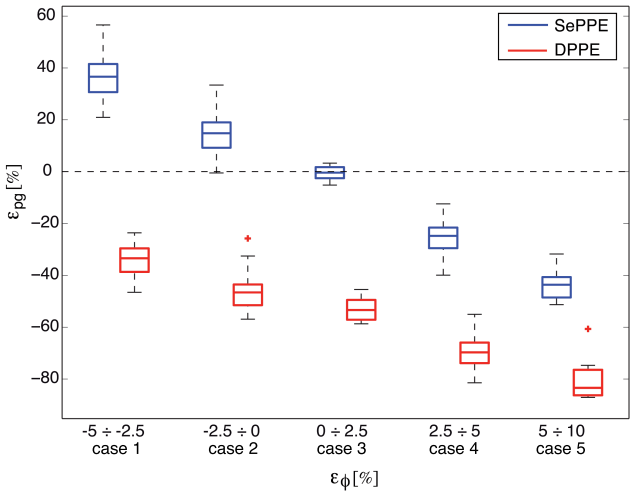

Fig. 3. Pressure gradient relative error for SePPE (blue) and DPPE (red) method. Moderate (case 1) and slight (case 2) lumen underestimation, slight (case 3), moderate (case 4) and high (case 5) lumen overestimation.

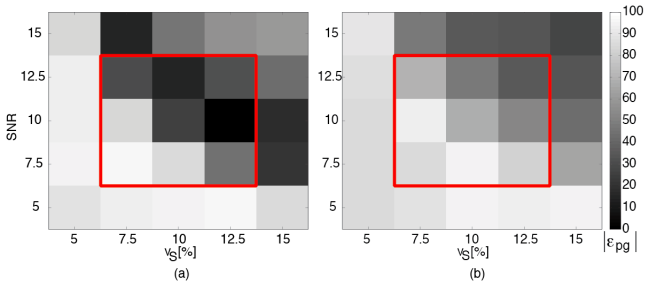

Fig. 4. Greyscale image of the absolute value of pressure gradient relative error as a function of v_S and SNR for SePPE (a) and DPPE (b).

In conclusion, we developed and tested a fully automatic method for a more reliable estimation of the laminar viscous pressure drop across systemic vessels from PC-MRI data.

ACKNOWLEDGMENT

The authors acknowledge financial support from the Department of Health, via the NIHR comprehensive Biomedical Research Centre award to Guys & St. Thomas NHS Foundation Trust in partnership with KCL and Kings College Hospital NHS Foundation Trust, and the Centre of Excellence in Medical Engineering funded by the WT and EPSRC under grant number WT 088641/Z/09/Z. Pablo Lamata holds a Sir Henry Dale Fellowship (grant number 099973/Z/12/Z).

REFERENCES

[1] D. S. Bach, “Unoperated Patients with Severe Aortic Stenosis”, J Am Coll Cardiol, vol. 50, 2018-19, 2007.
[2] F. Balleux-Buyens, “Velocity Encoding versus Acceleration Encoding for Pressure Gradient Estimation in MR Haemodynamic Studies”, Phys Med Biol, vol. 51, 4747-58, 2006.
[3] H. Baumgardtner, “Echocardiographic Assessment of Valve Stenosis: EAE/ASE Recommendations for Clinical Practice”, European Journal of Echocardiography, vol. 10, 1-25, 2009.
[4] H. Baumgardtner, “Overestimation of Catheter Gradients by Doppler Ultrasound in Patients with Aortic Stenosis: a Predictable Manifestation of Pressure Recovery”, J Am Coll Cardiol, vol. 33(6), 1655-61, 1999.
[5] J. Boch, “In Vivo Noninvasive 4D Pressure Difference Mapping in the Human Aorta: Phantom Comparison and Application in Healthy Volunteers and Patients”, Magn Reson Med, vol. 66, 1079-88, 2011.
[6] T. Ebbers, “Improving Computation of Cardiovascular Relative Pressure Fields From Velocity MRI”, Journal of Magnetic Resonance Imaging, vol. 30, 54-6, 2009.
[7] T. Feldman, “Assessment of the Transvalvular Pressure Gradient in Aortic Stenosis”, J Invasive Cardiol, vol. 18(8), 2006.
[8] S. Krittian, “A Finite-Element Approach to the Direct Computation of Relative Cardiovascular Pressure from Time-Resolved MR Velocity Data”, Medical Image Analysis, vol. 16, 1029-37, 2012.
[9] P. Lamata, “Aortic Relative Pressure Components Derived from 4D Flow Cardiovascular Magnetic Resonance”, Magn Reson Med, 2013.
[10] P. Lamata, “An Accurate, Fast and Robust Method to Generate Patient-Specific Cubic Hermite Meshes”, Medical Image Analysis, vol. 15, 801-813, 2011.
[11] S. Meier, “Non-invasive 4D Blood Flow and Pressure Quantification in Central Blood Vessels via PC-MRI”, Computing in Cardiology, 903-6, 2010.
[12] V. Mihalef, “Model-Based Estimation of 4D Relative Pressure Map from 4D Flow MR Images”, STACOM 2013, LNCS 8330, 236-243, 2014.
[13] A. de Vecchi, “Catheter-Induced Errors in Pressure Measurements in Vessels: an In-Vitro and Numerical Study”, IEEE Transactions on Biomedical Engineering, in print, 2014.